New pyrene and fluorene-based π-conjugated Schiff bases: Theoretical and experimental investigation of optical properties

YUNUSCAN SİVRİKAYA[1], HANDAN CAN SAKARYA[2]*, GÖKHAN KILIÇ[3],
SULTAN FUNDA EKTİ[4] and MERVE YANDIMOĞLU[2]

[1]*Graduate School of Natural and Applied Sciences, Eskişehir Osmangazi University, Eskişehir, Turkey,* [2]*Department of Chemistry, Faculty of Science, Eskişehir Osmangazi University, Eskişehir, Turkey,* [3]*Department of Physics, Faculty of Science, Eskişehir Osmangazi University, Eskişehir, Turkey and* [4]*Department of Chemistry, Faculty of Science, Eskişehir Technical University, Eskişehir, Turkey*

Abstract: The new Schiff bases with D-π-A system were synthesized by the reaction of polycyclic aldehydes and substituted benzothiazoles. The structures of the synthesized Schiff bases (**7a** and **9a**) were determined by FT-IR, ^{1}H--NMR, ^{13}C-NMR, ESI-Mass and elemental analyses. The optical properties of the new compounds were investigated and the optical band gaps (E_g) were calculated by the Tauc method using the UV–Vis absorption spectra. Density functional theory (DFT/B3LYP/6-31G(d,p)) calculations were conducted to get more insight on the structural and electronic properties of novel Schiff bases. The optimized molecular geometry, UV–Vis spectroscopic parameters and HOMO–LUMO energies were examined and the calculated results were compared with experimental data.

Keywords: imine; UV–Vis; optical bandgap; Tauc method; DFT.

INTRODUCTION

Schiff bases are compounds that are formed by the nucleophilic addition reaction of aldehydes or ketones and amines and contain the –CH=N– group in their structure. Schiff base was firstly synthesized by the chemist Hugo Schiff in Germany in 1894.[1] They are stable in the presence of aryl groups attached to imine group of the Schiff base.[2] It is known that Schiff base complexes containing aromatic rings are used in many different fields today. Since the imine group has strong bonds, Schiff bases are effectively used in the development of chemosensors.[3] At the same time, their complexes are versatile compounds used in qualitative and quantitative analyses, dyestuff, pharmaceutical and plastics indus-

---

1025

tries, synthesis of bioactive compounds, cycloaddition reactions and nucleophilic addition with organometallic reagents.[4–6] Schiff bases are used in pharmacological chemistry, pharmaceutical chemistry and especially in antibacterial,[7] antifungal[8] and antitumor[9] activity applications. Schiff bases have been investigated in recent years as functional material interesting optoelectronic properties due to their easily prepared and purified π-conjugated organic compounds.[10] New conjugated organic compounds with favorable optoelectronic properties offer significant advantages over carbon analogs as they can be easily prepared, purified[11] and synthesized without expensive catalysts. In previous studies, Schiff bases were used as optical molecular switches,[12] luminescence, pH indicators,[13] electrochromic and photochromic materials.[14] Schiff bases, which are isoelectronic with their vinyl bond, are a π-conjugated organic semiconductor material and form a kind of hole-transporting material.[15] The azomethine nitrogen of the Schiff base can be protonated with unshared electron pairs and organic and inorganic acids. In this way, the optical and electrooptical properties of azomethine compounds can be adjusted.[16] Organic materials play very important role in the field of nonlinear optics due to their delocalized electronic structure and are usually formed by bonding electron-donating and withdrawing groups from a π-electronic bridge with a large D-π-A conjugated system. The electron push––pull system helps to improve the molecular polarity so that larger nonlinear optical (NLO) materials can be obtained.[17] The electron-donating part in this system usually has been chosen as aromatic and heteroaromatic rings. These rings are great components for making tertiary NLO materials. In recent years, many studies have been conducted on the development of conjugated organic compounds.[18] Among π-conjugated organic compounds, especially Schiff base derivatives have emerged as promising compounds for NLO materials due to the π-electron bridge in carbon-nitrogen double bonds.[19] These compounds have very mobile clouds of π-electrons in the large molecular structures and can be easily polarized.[20]

In this study, we synthesized two new Schiff bases and their structures have been elucidated by various techniques such as ^{1}H-NMR, ^{13}C-NMR, ESI-Mass, and elemental analyses. The optical properties of these compounds have been investigated by UV–Vis spectroscopy. The band gap energies of the compounds have been determined by the UV–Vis absorption spectra using the Tauc method. Calculations of density functional theory (DFT) were performed using the Gaussian 09 program to investigate the optical properties of the compounds, and compare them for experimental data. DFT has been employed in theoretical studies to determine the vibrational frequencies, geometrical shapes and electrochemical characteristics of the molecule. In Schiff bases, the basic functional set of B3LYP/6-31G(d,p) was mostly preferred,[21,22] to explore the nature and type of UV–Vis shifts, a modified computation study time-dependent DFT was done.[23]

EXPERIMENTAL

General information

All chemicals and solvents were purchased from Sigma Aldrich. 2-Amino-4-methyl ben-zothiazole (97 %), pyrene-1-carbaldehyde (98 %), fluorene-2-carbaldehyde (99 %) and hydro-chloric acid (99.7 %) were used without further purification. The organic solvents (ethanol (EtOH, 99.8 %), dichloromethane (DCM, 99 %) and petroleum ether (90 %)) were used of HPLC grade or purified by a standard procedure. Melting points of synthesized compounds were determined by the Gallenkamp melting point apparatus using capillary tubes. FT-IR and UV–Vis absorption spectroscopy were taken at Eskisehir Osmangazi University Inorganic Chemistry Research Laboratory. FT-IR spectra were recorded with Bruker FT-IR spectro-meter in the range of 4000–400 cm^{-1} wavelengths. UV–Vis absorption spectra were recorded with a Shimadzu UV-2600 spectrometer and the optical band gap was determined using Tauc methods and evaluated using UV Probe Software. ^{1}H-NMR (500 MHz, DMSO-d_6, TMS internal standard) and ^{13}C-NMR (125 MHz, DMSO-d_6, TMS internal standard) spectroscopic analyses were carried out on using Jeol ECZ500R (11.75 Tesla) NMR equipment at Eskisehir Osmangazi University Central Research Laboratory Application and Research Center (ARUM). ESI-Mass and elemental analyses were recorded by Waters Alliance HPLC, 2Q micromass spectrometer, and Leco CHNS 932 elemental analyzer, respectively, at Ankara University Central Research Laboratory. Thin layer chromatography (TLC) plates were purchased as ready-coated from Merck and used to control the reactions. With the help of the hybrid funct-ional (B3LYP) and a specific basis set of 6-31G(d,p), a Gaussian 09 program was successfully operated. For extended electrochemical analyses of synthesized moieties, the energy gaps between their HOMO and LUMO states were determined using the readily available tool Gauss View 6.0.

*General method for 4-methyl-*N-*(pyren-1-yl-methylene) benzo[*d*]thiazol-2-amine (**7a**) and* N-*(9*H-*fluoren-3-yl-methylene)-4-methylbenzo[*d*]thiazol-2-amine (**9a**)*

A solution of 4-methyl-2-amino benzothiazole (1 eq.) in ethyl alcohol was added to appropriate aldehyde (0.8 eq), 2–3 drops of 5 % HCl solution were added to the reaction medium and refluxed in a nitrogen atmosphere at 75 °C for 4 h. The reaction was terminated with TLC control (1:10 petroleum ether/DCM). After cooling the solution at room tempera-ture overnight, the precipitates were filtered and extracted with DCM and then recrystallized from ethyl alcohol. **7a** was obtained as orange crystals and **9a** as yellow crystals. The protocol followed for the synthesis of the **7a** and **9a** Schiff bases and the numbering of the protons in the molecule is summarized in Scheme S-1 of the Supplementary material to this paper.

Analytical and spectral data of the synthesized compounds are given in Supplementary material.

RESULTS AND DISCUSSION

Chemistry

In the FT-IR spectra of compounds **7a** and **9a**, peaks at 3400 cm^{-1} belonging to the amino group of 4-methyl-2-amino benzothiazole, and at 1720 cm^{-1} belonging to the C=O group of aldehyde have not been observed. The imine group of compound **7a** is marked at 1593 cm^{-1}. The other peaks have been obs-erved at 3038 cm^{-1} (for aromatic C–H), 2965–2918 cm^{-1} (for aliphatic C–H), 1576, 1537 and 1478 cm^{-1} (for C=C peaks). Aromatic C–H, aliphatic C–H, aro-

matic C=C peaks have been observed at 3038, 2965–2918, 1576, 1537 and 1478 cm^{-1}, respectively (Fig. S-1 of the Supplementary material). The FT-IR spectrum of compound **9a** showed similar signals to the FT-IR spectrum of compound **7a** (Fig. S-3 of the Supplementary material).

According to ^{1}H-NMR spectrum compound **7a**, signals of 3 non-identical protons of the benzothiazole ring and 9 protons of the pyrene ring have been observed in the δ range of 8.15–9.28 ppm. Since the π-electrons in the pyrene ring of compound **7a** are conjugated with the imine group and are a donor group, the ring electrons are resonantly directed towards the benzothiazole ring (Fig. 1).
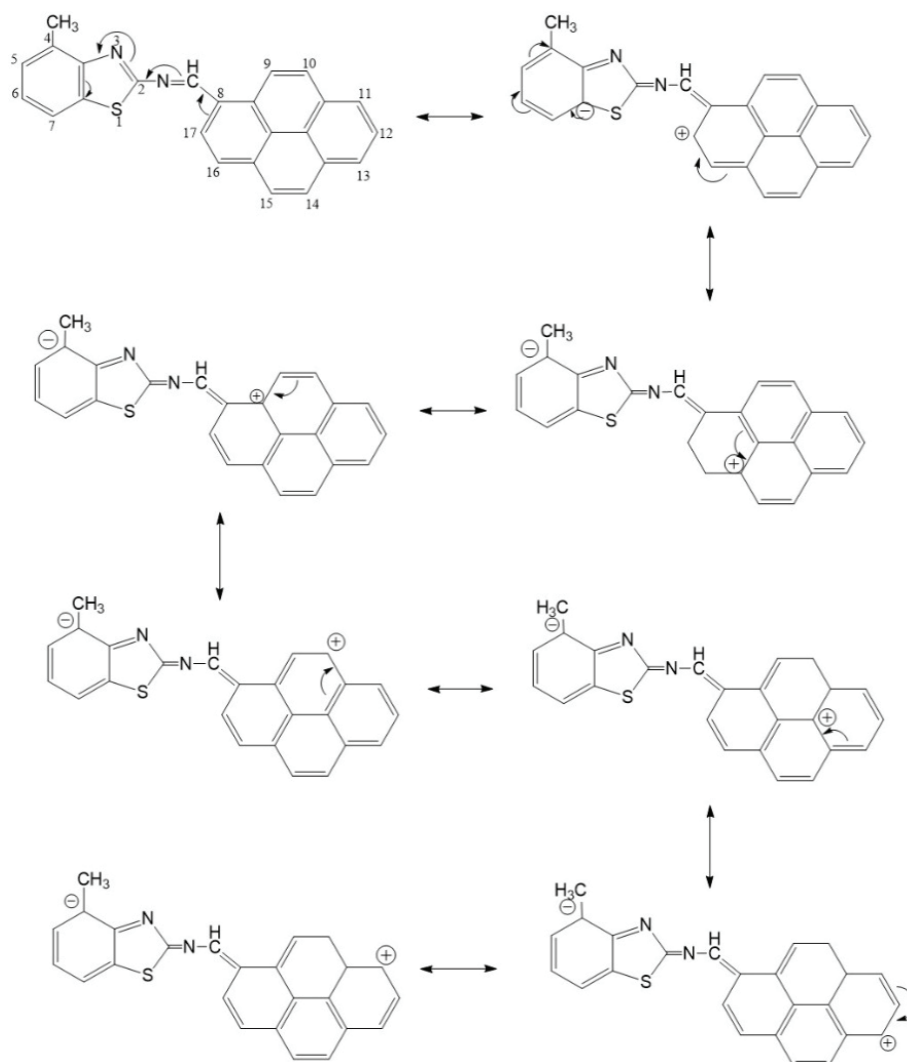

Fig. 1. Resonance forms of compound **7a**.

Therefore, considering the resonance structures of the compound **7a**, the protons in the pyrene ring have been observed, as expected, in the low field compared to the protons in the benzothiazole ring. As seen in Fig. S-2 of the Supplementary material, since the electron density around the H17 and H10 protons decreases with resonance, these protons resonate in the lower field due to the distance to the imine group (–CH=N–) compared to the other protons of pyrene ring. One proton doublets at δ 9.28 and 8.84 ppm have been observed as H17 and H10 protons, respectively. Other pyrene protons are marked at δ 8.44 ppm (*m*, 5H, H11, H16, H14, H15 and H9). One doublet at δ 8.28 ppm and one triplet at δ 8.15 ppm were observed belonging to H13 and H12 protons, respectively. On the other hand, the H5 and H7 protons of the acceptor benzothiazole ring are labeled as doublet at δ 7.31 ppm. Generally, the Schiff base imine proton resonates at δ 8–9 ppm, while the resonance delocalization of the π-electrons from the pyrene ring increases the polarization of the imine bond, and therefore the imine signal resonates at δ 9.98 ppm. In the ^{13}C-NMR of compound **7a**, 18 signals were observed instead of 23 signals of carbons in the aromatic region due to the identical carbons in the pyrene ring. In the ^{1}H-NMR spectrum of compound **9a**, it has been observed that the protons in the fluorene ring resonate at the higher field than substance **7a**, depending on the resonance structure (Fig. 2).
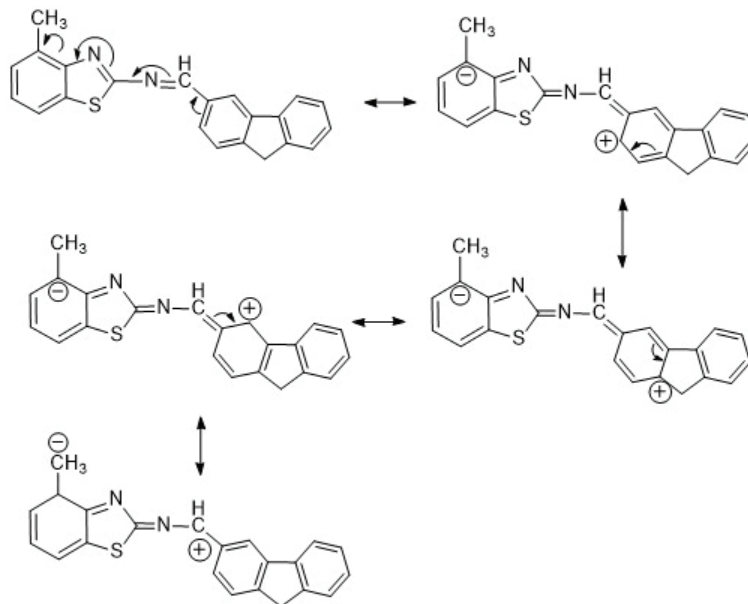

Fig. 2. Resonance forms of compound **9a**.

The ^{1}H-NMR of compound **9a** shows similar properties to compound **7a**. However, the increase in electron density around the protons in the fluorine ring

of compound **9a** lead these protons to resonate in the higher field, so the fluorene protons in compound **9a** resonate in higher field than the protons in the pyrene ring of compound **7a**. Therefore, the signal of the imine proton has been observed in the higher field at 9.14 ppm (Fig. S-4 of the Supplementary material).

In the ESI-MS spectrum of compound **7a**, the signal at *m/z* 377.68 (M⁺) is the peak of the molecular mass; *m/z* 165.15 and 245.48 are the signals of molecular masses of 4-methyl-2-amino benzothiazole and pyrenecarbaldehyde, respectively. M⁺+1, M⁺+2 peaks have been observed at *m/z* 378.71 and 379.77. In the ESI-MS spectrum of **9a**, the main peak of the compound has been observed at *m/z* 341.63 (M⁺). The peaks at *m/z* 342.63 and 343.65 belong to M⁺+1 and M⁺+2, respectively. The peaks of fluorene and benzothiazole ions have been observed at *m/z* 209 and 165.1, respectively.

The UV–Vis spectrum of material provides important structural information and a good way to study the properties of semiconductors, as it involves boosting an electron from the ground state from σ- and π-orbitals to the higher energy state.[24] It also gives information about the optical bandgap energy of the material. The forbidden energy gap of insulators is higher than 4 eV, whereas for semiconductors it is less than 3 eV.[25] In this study, solutions of Schiff bases **7a** and **9a** in different solvents, *n*-hexane, THF, DCM, DMF and DMSO have been prepared at 10^{-5} M concentrations and absorbance spectra has been recorded to clarify their optical properties. Two types of transitions, n–π* and π–π*, belonging to the imine group (–CH=N–), have been observed, as expected, in the UV–Vis spectrum of Schiff bases **7a** and **9a** (Fig. 3).
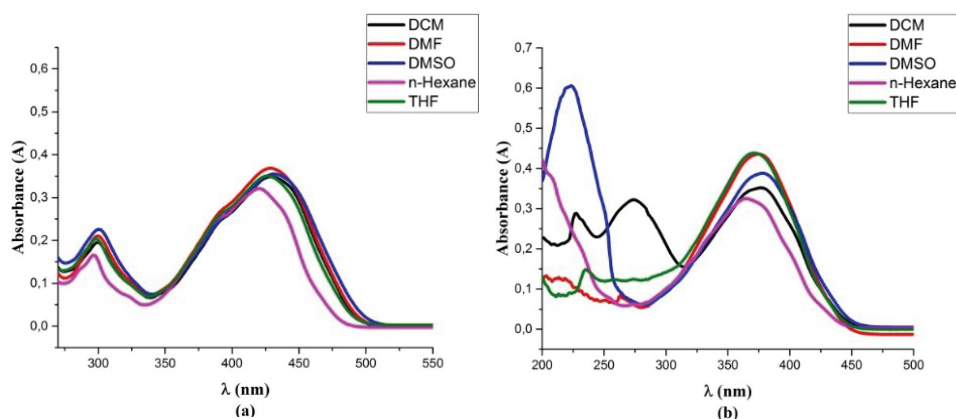

Fig. 3. a) UV–Vis spectra of compound **9a** in various solvents (1×10^{-5} M).

The short wavelength band results from electron conjugation on the backbone molecule and is known as the π–π* electronic transition. Long wavelength transitions are known as n–π* transitions as shown in Table I. This transition

occurs as a result of solute-solvent interaction *via* lone electron pair for compounds **7a** and **9a** (Figs. S-5 and S-6 of the Supplementary material).

TABLE I. The λ_{max} values (nm) of the n–π* and π–π* transitions of compounds **7a** and **9a** in different solvents

Compound	Transition type	*n*-Hexane	DCM	THF	DMF	DMSO
7a	n–π*	420	429	426	429	431
	π–π*	297	300	299	301	302
9a	n–π*	363	376	371	374	379
	π–π*	209	274	234	265	225

In the UV–Vis spectrum of compounds **7a** and **9a**, π–π* and n–π* transitions were observed to be red-shifted by solvent effect in five solvents with different polarities: *n*-hexane, THF, DCM, DMF and DMSO. This situation, as seen in Figs. 1 and 2, is due to the increased stability of the excited state by the conjugation effect. For the increase in the polarity of the solvent, the absorption band of the π–π* and n–π* transitions of compound **7a** was observed in the range of 297–302 nm and 420–431 nm, respectively. This situation is explained by increased stability of the excited state caused by conjugation, decrease of the energy of the excited state especially due to interaction with polar solvents, and a red shift of the π–π* transition as well as n–π* transition absorption band since the ground state energy does not change. Similarly, π–π* and n–π* transitions of compound **9a** are observed at 209–274 nm and 363–379 nm, respectively. With increasing solvent polarity, the n–π* transition of the imine of compound **9a** displays a red shift. However, a shift to a shorter wavelength has been observed due to decreasing conjugation in compound **9a** compared to compound **7a**. This red shift and high absorption in the UV–Vis regions is a desirable property in organic electronics.

Calculation of optical bandgap

Optical bandgaps in synthesized materials were calculated by the Tauc method.[26] Tauc describes the absorption coefficient dependence on photon energy as:

$$\alpha h\nu = A(h\nu - E_g)^n \tag{1}$$

Here, A is a constant, $h\nu$ is the photon energy, E_g is the optical bandgap. The value of *n* takes the value of 1/2 for direct transitions and 2 for indirect transitions. For direct transitions, the equation is given as:

$$\alpha n_0 h\nu \approx (h\nu - E_0)^{1/2} \tag{2}$$

This approach is valid for direct transitions. Here, *n* = 1/2 corresponds to the allowed direct transition. For indirect transitions, the equation is given as:

$$\alpha n_0 h\nu \approx (h\nu - E_0)^2 \qquad (3)$$

Here, $n = 2$ corresponds to possible allowed indirect transitions. Indirect transitions are generally valid for amorphous structures. Photon energies belonging to the wavelengths corresponding to the linear part of the curve in the absorption spectrum were calculated with the help of the $E = h\nu$ equation, and using these values, $(\alpha h\nu)^2$–$h\nu$ Tauc curves were drawn for each Schiff base separately for the direct allowed transition. The direct transition optical bandgaps of the Schiff bases is calculated from the value $(\alpha h\nu)^2 = 0$ of the line passing through the maximum number of points on the absorption edge of these curves. For a direct bandgap semiconductor, the optical bandgap is equal to the electronic bandgap. The graphs of $(\alpha h\nu)^2$–$h\nu$ of novel benzothiazole derived Schiff bases **7a** and **9a** are given in Figs. 4 and 5.
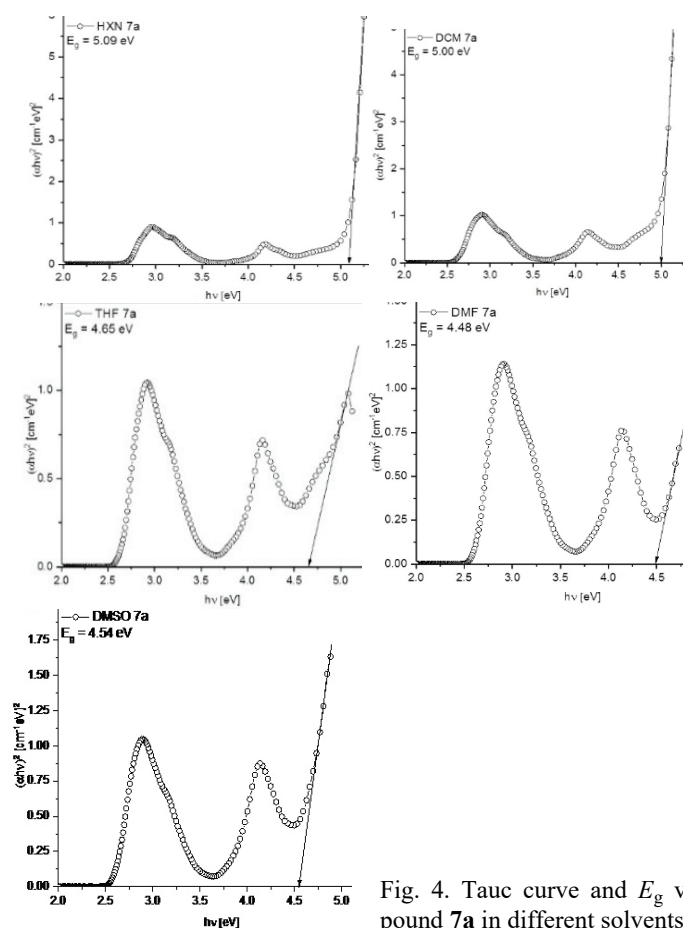

Fig. 4. Tauc curve and E_g values of compound **7a** in different solvents.
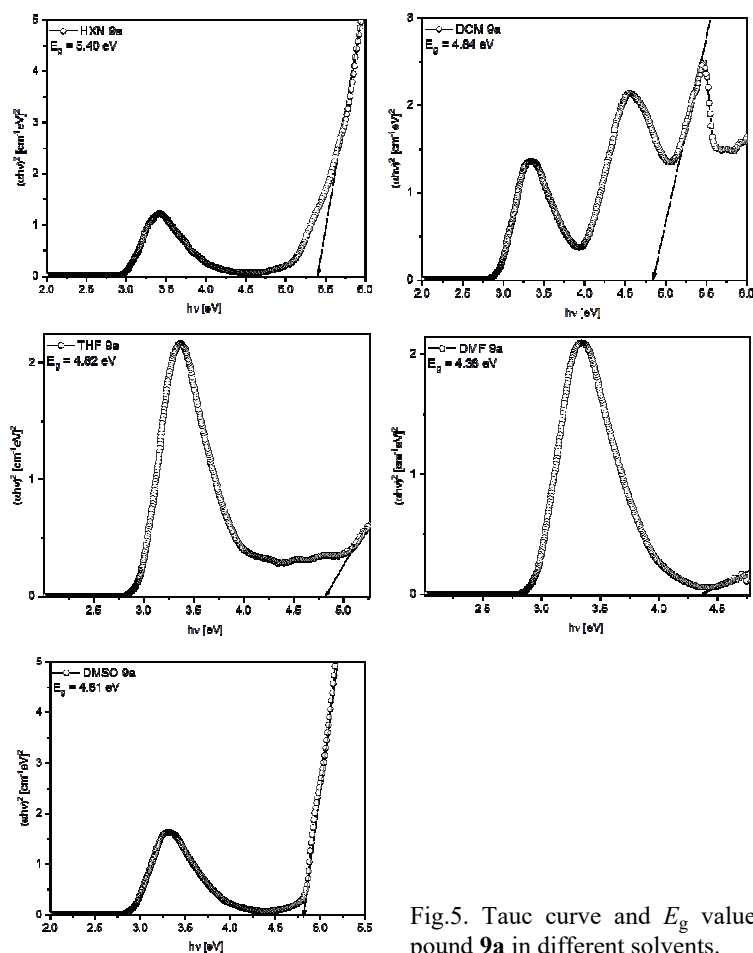
Fig.5. Tauc curve and E_g values of compound **9a** in different solvents.

The bandgap energy of organic π-conjugated semiconductors is related to the electronic structure of their molecules.[21,22,27,28] The effect, which increases the conjugation of organic compounds and solvent polarity, decreases the energy bandgap. Similarly, the difference in optical band gap E_g values of compounds **7a** and **9a** is due to their different resonance structures (Figs. 1 and 2). Due to the conjugation of the pyrene ring in compound **7a**, the optical bandgap energy (E_g) is smaller than in compound **9a**. The high bandgap energy of compound **9a** is due to the fluorene ring. The E_g values of Schiff base **7a** and **9a** showed variable values in solvents of different polarity (Table II).

The E_g of compound **7a** was decreased in polar solvents, particularly DMSO (4.54 eV) and DMF (4.48 eV) solvents. Although DMSO is more polar than DMF, the high E_g value was measured to be greater in the DMSO solvent. DMSO and DMF solvents are aprotic polar solvents, so there is no hydrogen

bond interaction with compound **7a**. This increase in the optical bandgap energy E_g value was explained by the increase in the molecular mass of DMSO. Due to the trapping of electrons and holes, the bandgap energy between the valence band and conduction band increases as the particle size decreases The optical bandgap energy E_g decreases gradually with chain length. Therefore, when the E_g values of **7a** and **9a** are compared, the decrease in the E_g values of **9a** is due to the smaller particle size.

TABLE II. Optical bandgap energy (E_g / eV) of compound **7a** and **9a**

Compound	*n*-Hexane	DCM	THF	DMF	DMSO
7a	5.09	5.00	4.65	4.48	4.54
9a	5.40	4.84	4.82	4.38	4.81

Computational study

An extensive body of research supports the idea that DFT calculation shed light on the structural and electronic properties of conjugated molecules.[21,22] In Schiff bases, the B3LYP/6-31G(d,p) basis functional set was mostly preferred to investigate the nature and type of UV–Vis shifts, and a modified computational study of time-dependent DFT (TD-DFT) was conducted. This function, particularly adept at accurately calculating electron distribution and energy levels in conjugated systems, facilitates the reliable modeling of molecular structures and spectroscopic properties.[21–23] In this way, the ground state optimization of compound **7a** and **9a** were performed at the B3LYP/6-31G(d,p) level in the gas phase and DMSO without any symmetry constraints employing the Gaussian09 package program.[29,30] Optimization was first performed by scanning the potential energy surface (PES) and selecting the geometry around zero. Following the optimization with B3LYP, vibration frequency calculations were performed at the same level of theory and the minima of the calculated structures were verified by analyzing the harmonic vibrational frequencies using analytical second derivatives, which have *NIMAG* = 0. The conductor-like polarizable continuum model (CPCM) was implemented to discern the solvent effect in DMSO.[27,31] The construction of frontier molecular orbitals (FMO) was completed using Gausview[28] while the dihedral angle between benzothiazole and the pyrene ring is 174° in compound **7a**, the dihedral angle between benzothiazole plane and fluorene is 180° in compound **9a**. The angles indicated that pyrene and fluorene rings are planar with the benzotiazole plane in **7a** and **9a**. The dihedral angles of the related atoms are given in detail in the supporting information.

To reach more insight into intramolecular charge transfer (ICT) characters of the compounds frontier molecular orbitals (FMO) were calculated. The HOMOs were found to be, in both **7a** and **9a**, localized on benzothiazole, azomethine bonds and the rings (pyrene in **7a**, fluorene in **9a**). Concerning the LUMOs, they

were localized on the azomethine bonds, pyrene (**7a**) and fluorene (**9a**) rings spreading slightly over benzothiazole. As demonstrated in Fig. 6, the azomethine bond is a π-bridge between the benzothiazole and the rings in compound **7a** and **9a.** λ_{max} values and vertical excitation energies of the compounds were predicted by a time-dependent DFT (TD-DFT) method.
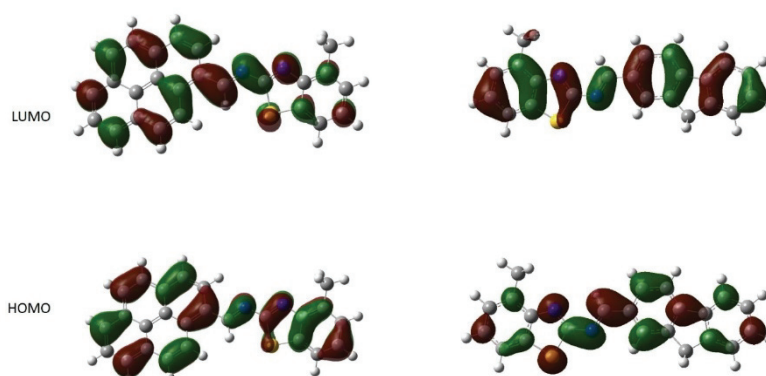

Fig. 6. HOMOs and LUMOs of **7a** (left) and **9a** (right) estimated at the B3LYP/6-31G(d,p) level in the gas phase.

In order to receive absorption bands, N states of 50 for singlets were computed. The λ_{max} values of compounds **7a** and **9a** are predicted to be 431.8 and 388.56 nm in DMSO, which shows low energy transitions resulting from HOMO–LUMO (95–98 %). The calculated excitation and absorption energies agree well with the experimental results.

In parallel with all calculations performed, a dispersion component was added to the B3LYP 6-31G(d,p) level of theory used in DFT calculations, and re-optimization and frequency calculations of the investigated **7a** and **9a** molecules were completed. First, there is no difference in the dihedral angles and therefore the geometry of the optimized structures by using the dispersion component.

Excited energy calculations were rerun with the freshly optimized geometries, and results were compared with previously obtained theoretical results. When the HOMO–LUMO band gap energies of **7a** and **9a** were examined, narrower band gap energies were detected compared to the calculations conducted without using this dispersion component. The band gap energy values obtained both without and using the dispersion component tend to decrease or increase in the same way as the experimental study. However, it is seen that the band gap value obtained by adding the dispersion component deviates further from the experimental data. The results of the calculations with and without the dispersion component are given in supporting information.

CONCLUSION

In this study, we have synthesized and characterized two novel Schiff bases **7a** and **9a**. Optical properties have been investigated by UV–Vis spectra. The optical bandgap has been calculated by the Tauc method and DFT calculation. The optical band gap of compounds **7a** and **9a** in the DMF solvent is 4.48 and 4.38 eV, respectively. Experimental results showed that the optical band gap of compounds **7a** and **9a** decreases with increasing optical absorption, red-shift, π-electronic system, solvent polarity and particle size. Finally, the increased optical absorption and reduced energy gap make the optimized samples suitable materials for solar applications.

Since pyrene contributes more to conjugation than fluorene, the experimental band gap energy of compound **7a** is expected to be lower than that of compound **9a**. This difference was observed as 2.87 eV for **7a** and 3.19 eV for **9a** in calculated data conducted in DMSO by B3LYP 6-31G(d,p). Considering the optical band gap energy obtained by the Tauc method from the experimental absorbance graphs recorded in DMSO (4,54 eV for **7a** and 4.81 eV for **9a**), the trends in the calculated band gap energies are in agreement with the experimental data. In addition, when the frontier molecular orbital is examined, it is clearly seen that the electrons are not located in only one region, but that these electrons are homogeneously distributed throughout the molecule. The fact that the charge transport in the molecule can continue unhindered throughout the molecule can be explained by the fact that compounds **7a** and **9a** have almost planar structures. For future studies, molecules with narrow band gap energies can be designed and synthesized by increasing the conjugated groups attached to compounds **7a** and **9a**.

SUPPLEMENTARY MATERIAL

Additional data are available electronically at the pages of journal website: https://www.shd-pub.org.rs/index.php/JSCS/article/view/12546, or from the corresponding author on request.

ИЗВОД
НОВЕ π-КОЊУГОВАНЕ ШИФОВЕ БАЗА ЗАСНОВАНЕ НА ПИРЕНУ И ФЛУОРЕНУ: ТЕОРИЈСКО И ЕКСПЕРИМЕНТАЛНО ИСТРАЖИВАЊЕ ОПТИЧКИХ СВОЈСТАВА

YUNUSCAN SİVRİKAYA[1], HANDAN CAN SAKARYA[2], GÖKHAN KILIÇ[3], SULTAN FUNDA EKTİ[4] и MERVE YANDIMOĞLU[2]

[1]*Graduate School of Natural and Applied Sciences, Eskişehir Osmangazi University, Eskişehir, Turkey,*
[2]*Department of Chemistry, Faculty of Science, Eskişehir Osmangazi University, Eskişehir, Turkey,*
[3]*Department of Physics, Faculty of Science, Eskişehir Osmangazi University, Eskişehir, Turkey u*
[4]*Department of Chemistry, Faculty of Science, Eskişehir Technical University, Eskişehir, Turkey*

Реакцијом полицикличних алдехида и супституисаних бензотиазола, синтетисане су нове Шифове базе са D-π-A системом. Структуре синтетисаних Шифових база (**7a** и

9a) одређене су помоћу FT-IR, ^{1}H-NMR, ^{13}C-NMR, ESI-Mass и елементалном анализом. Истражене су оптичке особине нових једињења и оптички јаз између трака (E_g) је израчунат Тауковом методом користећи UV–Vis апсорпционе спектре. Да би се добио бољи увид у структурне и електронске особине нових база урађена су израчунавања теоријом функционала густине (DFT/B3LYP/6-31G(d,p)). Оптимизоване молекулске гео-метрије, UV–Vis спектроскопски параметри и HOMO–LUMO енергије су испитане и резултати израчунавања су упоређени са експерименталним подацима.

REFERENCES

1. H. Schiff, *Justus Liebigs Ann. Chem.* **150** (1869) 193
2. N. Öztürk, *MSc Thesis*, Istanbul University, 1998
3. C. Sasaki, K. Nakajima, M. Kojima, J. Fujita, *Bull. Chem. Soc. Jpn.* **64** (1991) 1318 (https://doi.org/10.1246/bcsj.64.1318)
4. S. Kanemasa, M. Yoshioka, O. Tsuge, *Bull. Chem. Soc. Jpn.* **62** (1989) 869 (https://doi.org/10.1246/bcsj.62.869)
5. M. F. Aly, M. I. Younes, S. A. Metwally, *Tetrahedron* **50** (1994) 3159 (https://doi.org/10.1016/S0040-4020(01)81114-5)
6. A. E. Taggi, A. M. Hafez, H. Wack, B. Young, D. Ferraris, T. Lectka, *J. Am. Chem. Soc.* **124** (2002) 6626 (https://doi.org/10.1021/ja0258226)
7. K. Singh, M. S. Barwa, P. Tyagi, *Eur. J. Med. Chem.* **41** (2006) 147 (https://doi.org/10.1016/j.ejmech.2005.06.006)
8. S. K. Sridhar, M. Saravanan, A. Ramesh, *Eur. J. Med. Chem.* **36** (2001) 615 (https://doi.org/10.1016/S0223-5234(01)01255-7)
9. R. Mladenova, M. Ignatova, N. Manolova, T. Petrova, I. Rashkov, *Eur. Polym. J.* **38** (2002) 989 (https://doi.org/10.1016/S0014-3057(01)00260-9)
10. M. Koole, R. Frisenda, M. L. Petrus, M. L. Perrin, H. S. van der Zant, T. J. Dingemans, *Org. Electron.* **34** (2016) 38 (https://doi.org/10.1016/j.orgel.2016.03.043)
11. N. Bouguerra, A. Růžička, C. Ulbricht, C. Enengl, S. Enengl, V. Pokorná, D. Výprachtický, E. Tordin, R. Aitout, V. Cimrová, D. A. M. Egbe, *Macromolecules* **49** (2016) 455 (https://doi.org/10.1021/acs.macromol.5b02267)
12. J. Jankowska, M. F. Rode, J. Sadlej, A. L. Sobolewski, *ChemPhysChem* **13** (2012) 4287 (https://doi.org/10.1002/cphc.201200560)
13. K. Haupt, K. Mosbach, *Chem. Rev.* **100** (2000) 2495 (https://doi.org/10.1021/cr990099w)
14. S. Pu, Z. Tong, G. Liu, R. Wang, *J. Mater. Chem. C* **1** (2013) 4726 (https://doi.org/10.1039/C3TC30804A)
15. M. Petrus, R. Bouwer, U. Lafont, S. Athanasopoulos, N. Greenham, T. Dingemans, *J. Mater. Chem. A* **2** (2014) 9474 (https://doi.org/10.1039/C4TA01629G)
16. A. Bolduc, L. Rivier, S. Dufresne, W. Skene, *Mater. Chem. Phys.* **132** (2012) 722 (https://doi.org/10.1016/j.matchemphys.2011.12.002)
17. U. H. A. Azeez, D. Ayyappan, S. G. Chidambaram T, R. Singh, J. Subbiah, A. Sambandam, *J. Mol. Struct.* **1294** (2023) 136315 (https://doi.org/10.1016/j.molstruc.2023.136315)
18. S. Mukhopadhyay, C. Risko, S. R. Marder, J.-L. Brédas, *Chem. Sci.* **3** (2012) 3103 (https://doi.org/10.1039/C2SC20861J)
19. Z. Fatima, H. A. Basha, S. A. Khan, *J. Mol. Struct.* **1292** (2023) 136062 (https://doi.org/10.1016/j.molstruc.2023.136062)

20. W. Xu, Z. Shao, Y. Han, W. Wang, Y. Song, H. Hou, *Dyes Pigm*. **152** (2018) 171179 (https://doi.org/10.1016/j.dyepig.2018.01.056)
21. G. Turkoglu, M. Cinar, A. Buyruk, E. Tekin, S. Mucur, K. Kaya, T. Ozturk, *J. Mater. Chem. C* **4** (2016) 6045 (https://doi.org/10.1039/C6TC01285J)
22. M. Wałęsa-Chorab, M. H. Tremblay, W. G. Skene, *Chem. Eur. J.* **22** (2016) 11382 (https://doi.org/10.1002/chem.201600859)
23. K. S. M. Salih, *J. Mol. Struct.* **1244** (2021) 131267 (https://doi.org/10.1016/j.molstruc.2021.131267)
24. K. Mangaiyarkarasi, A. Ravichandran, K. Anitha, A. Manivel, *J. Mol. Struct*. **1155** (2018) 758 (https://doi.org/10.1016/j.molstruc.2017.11.065)
25. G. A. Evingür, Ö. Pekcan, *Compos. Struct*. **183** (2018) 212 (https://doi.org/10.1016/j.compstruct.2017.02.058)
26. J. Singh, K. Shimakawa, in *Advances in Amorphous Semiconductors*, J. Singh, K. Shimakawa, Eds., Taylor and Francis New York, 2003 (ISBN 9780415287708)
27. M. Cossi, N. Rega, G. Scalmani, V. Barone, *J. Comput. Chem*. **24** (2003) 669 (https://doi.org/10.1002/jcc.10189)
28. R. Dennington, T. Keith, J. Millam, *J.GaussView*, *version* 5, Semichem Inc., Shawnee Mission, KS, 2009
29. C. Lee, W. Yang, R.G. Parr, *Phys. Rev., B* **37** (1988) 785 (https://doi.org/10.1103/PhysRevB.37.785)
30. *Gaussian 09, Rev. A*, Gaussian Inc, Wallingford, CT, 2009
31. V. Barone, M. Cossi, *J. Phys. Chem*., *A* **102** (1998) 1995. (https://doi.org/10.1021/jp9716997).